BMC Medical Informatics and Decision Making

RESEARCH

Open Access

Analysis of anterior segment in primary angle closure suspect with deep learning models

Ziwei Fu[1,2,3], Jinwei Xi[1], Zhi Ji[1,2], Ruxue Zhang[4], Jianping Wang[5], Rui Shi[5], Xiaoli Pu[6], Jingni Yu[7], Fang Xue[2], Jianrong Liu[7], Yanrong Wang[8], Hua Zhong[9], Jun Feng[4], Min Zhang[4*] and Yuan He[1,2,3*]

Abstract

Objective To analyze primary angle closure suspect (PACS) patients' anatomical characteristics of anterior chamber configuration, and to establish artificial intelligence (AI)-aided diagnostic system for PACS screening.

Methods A total of 1668 scans of 839 patients were included in this cross-sectional study. The subjects were divided into two groups: PACS group and normal group. With anterior segment optical coherence tomography scans, the anatomical diversity between two groups was compared, and anterior segment structure features of PACS were extracted. Then, AI-aided diagnostic system was constructed, which based different algorithms such as classification and regression tree (CART), random forest (RF), logistic regression (LR), VGG-16 and Alexnet. Then the diagnostic efficiencies of different algorithms were evaluated, and compared with junior physicians and experienced ophthalmologists.

Results RF [sensitivity (Se) = 0.84; specificity (Sp) = 0.92; positive predict value (PPV) = 0.82; negative predict value (NPV) = 0.95; area under the curve (AUC) = 0.90] and CART (Se = 0.76, Sp = 0.93, PPV = 0.85, NPV = 0.92, AUC = 0.90) showed better performance than LR (Se = 0.68, Sp = 0.91, PPV = 0.79, NPV = 0.90, AUC = 0.86). In convolutional neural networks (CNN), Alexnet (Se = 0.83, Sp = 0.95, PPV = 0.92, NPV = 0.87, AUC = 0.85) was better than VGG-16 (Se = 0.84, Sp = 0.90, PPV = 0.85, NPV = 0.90, AUC = 0.79). The performance of 2 CNN algorithms was better than 5 junior physicians, and the mean value of diagnostic indicators of 2 CNN algorithm was similar to experienced ophthalmologists.

Conclusion PACS patients have distinct anatomical characteristics compared with health controls. AI models for PACS screening are reliable and powerful, equivalent to experienced ophthalmologists.

Keywords Primary angle closure suspect, Anatomical characteristics, Machine learning, Convolutional neural network, Screening

*Correspondence:
Min Zhang
dr.zhangmin@nwu.edu.cn
Yuan He
heyuan@xiyi.edu.cn
[1]The Second Affiliated Hospital of Xi'an Medical University, Xi'an, Shaanxi 710038, China
[2]Xi'an Medical University, Xi'an, Shaanxi 710021, China
[3]Xi'an Key Laboratory for the Prevention and Treatment of Eye and Brain Neurological Related Diseases, Xi'an, Shaanxi 710038, China
[4]School of Mathematics, Northwest University, Xi'an 710127, China
[5]Shaanxi Provincial People's Hospital, Xi'an, Shaanxi 710068, China
[6]Xianyang First People's Hospital, Xianyang, Shaanxi Province 712000, China
[7]Xi'an People's Hospital, Xi'an, Shaanxi 712099, China
[8]Yan'an People's Hospital, Yan'an, Shaanxi 716099, China
[9]The First Affiliated Hospital of Kunming Medical University, Kunming, Yunnan Province 650032, China

Introduction

Glaucoma is the second blindness disease in the world. The abnormal anatomical structure is the main cause, which leads to outflow of aqueous humor blocked. The pathological high intraocular pressure (IOP) brings about loss of visual field and irreversible damage of optic nerve [1]. In 2013, the number of primary angle closure glaucoma (PACG) patients reached 23.36 million worldwide. It is estimated that there will be 32.04 million PACG patients in 2040, 87% of which will be from Asia [2, 3].

The International Society of Geographical and Epidemiological Ophthalmology (ISGEO) delimits three stages of the pathogenesis of PACG: primary angle closure suspect (PACS), primary angle closure (PAC) and PACG [4]. PACS shows normal intraocular pressure (IOP), non-peripheral synechia, and iridotrabecular contact (ITC) ≥ 180° [4]. PAC possessed some pathological anatomical characteristics such as thick cornea [5], pleated or bulging iris [6], thick or anteriorly positioned lenses [7], narrow or shallow anterior chamber [7]. Those features are also present in PACS [8]. Laser perioridectomy for patients with PACS can reduce the risk of angle closure progression [9].

Population screening is beneficial, which can diagnose disease and manage patients at the earliest stage [10]. For PACS screening, the devices include gonioscopy, anterior segment optical coherence tomography (AS-OCT) and others. Gonioscopy is gold standard for diagnosis, however the accuracy is affected by the operating of the technician and the cooperation of the subjects; strong light and excessive pressure may cause false results, and the contact between lens and cornea often brings discomfort and risk for patients [11]. AS-OCT is an optical imaging technique, which is widely used for anterior segment screening in clinical practice. The advantages of AS-OCT include rapidity, non-invasiveness, high resolution and high consistency. The diagnostic results showed a correlation between AS-OCT and gonioscopy [12]. Importantly, when angle changes from wide to narrow, AS-OCT is more sensitive than gonioscopy [13]. So AS-OCT is a promising tool for PACS screening.

In recent years, artificial intelligence (AI) shows tremendous application foreground in auxiliary diagnosing, which meets screening requirements of sensitivity, specificity, objectivity, cost, convenience [14, 15]. Several studies report deep learning models are expert in angle classification, and the diagnostic performance reaches professional level [16, 17].

Screening for PACS in a large population is labor-intensive and inefficient. Inexperienced physicians have low diagnostic accuracy, and staff are susceptible to environmental and attention influences, resulting in erratic results. AI technology can compensate for these shortcomings. In this study, to analyze PACS patients' anatomical characteristics of anterior chamber configuration, and to establish AI-aided diagnostic system for PACS screening, we enrolled 839 subjects from multiple medical centers, with 1668 AS-OCT scans, to compare the anatomical characteristics between normal subjects and PACS. Different AI models were trained with machine learning algorithms and convolutional neural network (CNN) approaches, and their performances to screen PACS were compared. Their performances were also compared with junior physicians and experienced ophthalmologists. Finally, the application prospect of these models, the advantages and limitations of the present work, were discussed.

Methods

Data preparation

This study adhered to the guidelines of *Declaration of Helsinki*, and approved by the Ethics Committee of the Second Affiliated Hospital of Xi'an Medical College. Patients who accepted AS-OCT examination in the hospital, from September 2019 to January 2022, were enrolled. All subjects understood the research content and signed informed consent document voluntarily.

Inclusion criteria for normal control group are as follows: (1) Age > 40 years old; (2) Best corrected visual acuity (BCVA) [Log minimum angle resolution (MAR)] ≤ 0.3; (3) Diopter < 3.00 D, binocular difference ≤ 1.00 D; (4) 21 ≤ axial length (AL) ≤ 25 mm, binocular difference ≤ 0.5 mm; (5) IOP < 21 mmHg;

Inclusion criteria for the PACS group are as follows: (1) the examined eye didn't appear clinical symptoms and the fellow eye had an episode of primary angle closure; (2) there were anatomical features of PACG such as shallow anterior chamber and narrow angle; (3) ITC > 180° under gonioscopy; (4) there was no peripheral synechia. Exclusion criteria are as follows: (1) IOP ≥ 21 mmHg; (2) a history of glaucomatous attack with structural damage; (3) glaucoma led to visual field loss or fundus damaged; (4) some drugs which affected anterior segment structure or aqueous humor circulation were used or being used; (5) patients suffered from diseases affecting anterior segment structure; (6) history of trauma, surgery, and laser treatment; (7) poor cooperation with inspection; (8) AS-OCT image with poor quality. All subjects underwent standardized ophthalmic examination including LogMAR chart, Auto-Refractor, slitlamp microscope, Goldmann applanation tonometer, ophthalmoscope, intraocular len-master, ophthalmic ultrasonography, automatic perimetry, gonioscope, and AS-OCT.

Image acquisition and data measurement

Operation of AS-OCT was accomplished by the same expert technician. Patients sat on the chair in natural light, whose eyes are opened as much as possible.

Operator scanned anterior segment by 16 mm wide-angle lens under specific mode, and moved focus to the center of anterior chamber. When the structure of anterior chamber was presented clearly, the operator captured image by 1310 nm near-infrared laser. The frequency of volume scanning was 30,000 Hz, range was 16 mm, depth was 6 mm. lens' vertical resolution was 10 μm, and the horizontal resolution was 30 μm. After shooting, the image obtained was divided automatically into 360° sites according to clockwise direction. The scans of 180° and 0° sites were selected to observed, for that the influence of eyelid extrusion and personal errors was minimal. The quality of every scan must be enough for making a diagnosis, before stored with non-destructive PNG format. The evaluation included three indicators: centered position of shooting; complete structure of anterior chamber; clear structure of cornea, sclera, iris, chamber angle and lens. The position of the scleral spur was determined independently by three ophthalmologist. If the result was not certain, it would be handed over to the fourth ophthalmologist for judgment. Finally, we use the instrument's software to measure anterior chamber parameters: anterior chamber depth (ACD), central corneal thickness (CCT), anterior chamber width (ACW), lens dome (LV), the angle of opening distance at 500 μm (AOD500), angle opening distance at 750 μm (AOD750), corneal recess area at 500 μm (ARA500), corneal recess area at 750 μm (ARA750), trabecular inter-iris area at 500 μm (TISA500), trabecular inter-iris area at 750 μm (TISA750), the angle between the trabecular iris at 500 μm (TIA500), the angle between the trabecular iris at 750 μm (TIA750).

Design of artificial intelligence (AI) approaches to screen PACS

The AS-OCT scan was cut into two halves with mid-axis of anterior chamber, then each part was mirror-flipped along the cutting edge to compound complete scan. Three machine learning algorithms and two CNN approaches were constructed on the 12 parameters and the scans to diagnose PACS, respectively. 10-fold cross-validation or 5-fold cross-validation was applied to evaluate the performance of the AI models. The performance of the models were tested, and compared based on sensitivity (Se), specificity (Sp), positive predictive value (PPV), negative predictive value (NPV), and area under curve (AUC). The proposed methods were implemented on the PyTorch platform and trained with a single NVIDIA GeForce RTX3090 GUP. The time consumption for the training for the model based on machine learning algorithms was less than 1 min, and that for the model based on CNN approaches was less than 2 h.

1) The classification and regression tree (CART) algorithm is applied for decision tree method, which the Gini index is adopted for dividing indicators. Starting from the root node, the Gini index is calculated after all features are divided into the training sample. The feature with the smallest Gini index value is selected as the optimal bisection feature and optimal segmentation point of the training set, and the data of this node are divided into left and right nodes. The above steps are repeated for recursive division. When the number of node samples or the Gini index is less than the threshold, the classification result is obtained, that is, the leaf node [18, 19].
2) The random forest (RF) method belongs to the integrated machine learning algorithm, and bootstrap sampled method is used for training model. Each training sample had multiple features. When a node is split, one optimal feature is selected as the split feature until it could not be split, and the leaf node category is obtained. Multiple intact trees are constituted random forest method. The bagging method is applied for result prediction, and the most categories are the final results [20].
3) Logistic regression (LR) as a classical classification method, belongs to log linear model, which is expressed by conditional probability distribution. In the conditional probability distribution, the random variable is the input (i.e., real number), the random variable is set as the output with a value of 1 or 0. For a given X, the conditional probability value could be obtained. X belongs to the category with a large probability value. It is used to solve the problem of "yes" or "no" in two classifications. It had the advantages of simplicity and fast training speed [21].
4) CNN is a kind of neural network with multi-layer depth structure in DL algorithm, which can perform convolution operation. It uses the existing model training network to realize the mapping from original input to output label, and is often used to analyze visual images. VGG net (visual geometry group, VGG) architecture includes 16 layers of weight parameters. VGG-16 model is composed of 13 convolution layers, 5 pooling layers and 3 full connection layers. Unified setting: 3×3-size convolution kernel, step size of 1, same filling, 2×2 maximum pooled nuclei in steps of 2 [22] (Fig. 1).
5) The architecture of Alexnet uses two service processors, consisting of five convolution layers and three full connection layers. Each convolution layer introduces the excitation function relu, which accelerates the convergence speed of the model and enhances the nonlinear mapping ability. At the same time, local corresponding homogenization

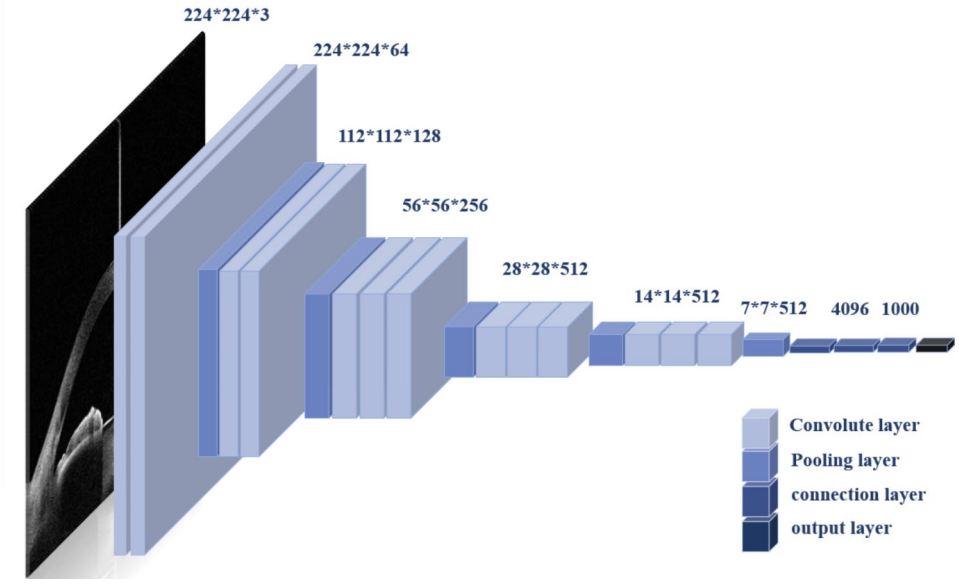

Fig. 1 Structure of VGG16

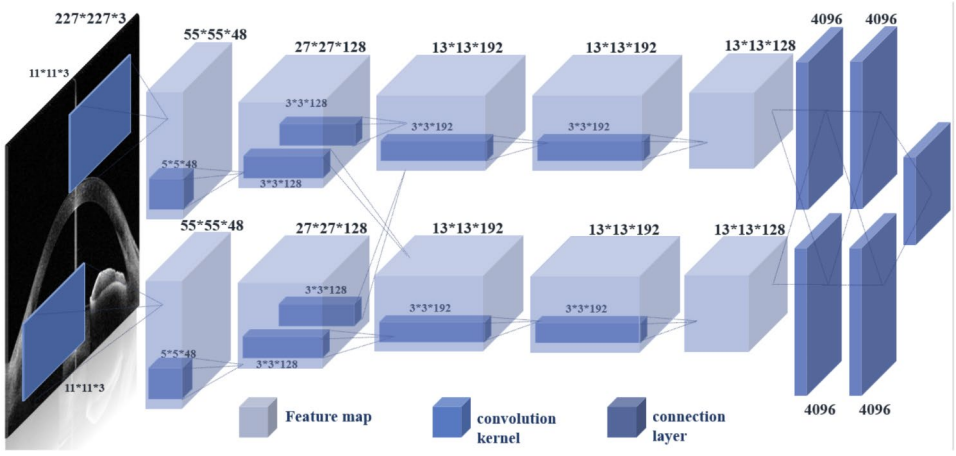

Fig. 2 Structure of Alexnet

processing (LRN) is carried out to help model generalization. The pool processing adopts the maximum pool that can be covered. In the full connection layer, dropout method is used to ignore some neural nodes to reduce over-fitting phenomenon [23] (Fig. 2).

Comparison of the diagnostic ability between physicians and digital approaches

The test set of CNN was hided classified labels and patient-related information for conducting contest with physicians. After same training, 5 junior ophthalmologists were selected randomly. When each ophthalmologist made the diagnosis independently, tester recorded results. Next, two ophthalmologists who specialized in glaucoma more than 10 years were invited to diagnose PACS professionally. All results were compared with CNN model.

Statistical analysis

The diagnostic results included four parameters: true positive (TP), false positive (FP), false negative (FN), true negative (TN). Se, Sp, PPV, NPV, and AUC were accordingly calculated (Table 1). GraphPad Prism 8.0 (Graphpad software, La Jolla, CA, USA) was applied for statistical analyzing. Chi-square test or independent sample t test was used for data analysis. When P value < 0.05, the difference was statistically significant.

Results

Subjects' characteristics

In this study, a total of 839 subjects from 5 medical centers were enrolled, with 1668 OCT scans. Most of

Table 1 The mathematical equations used for the evaluation metrics

	Mathematical euations
Se	TP / (TP + FN)
Sp	TN / (FP + TN)
PPV	TP / (FP + TP)
NPV	TN / (FN + TN)
AUC	$AUC=[\sum_{i\in positive\ class} ranki-M\times(M+1)/2]/(M\times N)$

Se: sensitivity; Sp: specificity; PPV: positive predictive value; NPV: negative predictive value; AUC: area under curve; TP: true positive; FN: false negative; TN: true negative; FP: false positive; i, the number of the sample after the probability scores of all samples were ranked from smallest to largest; M, the number of postive sample; N, the number of negative sample

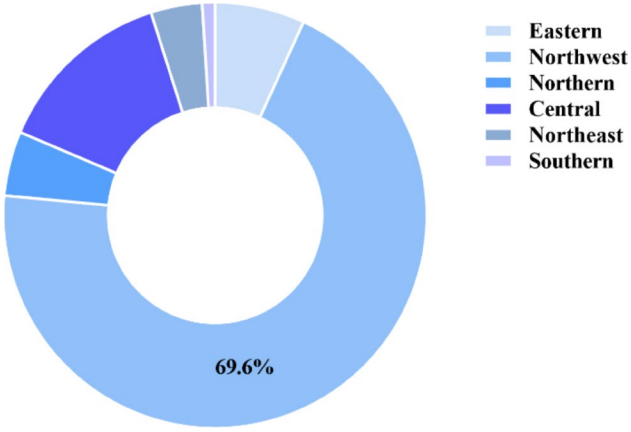

Fig. 3 Most of subjects came from the Northwest China, accounted for 69.60%, and 30.49% were from other regions

Table 2 Biometric data of subjects in PACS group and normal group

		Normal Group	PACS Group	*P* Value
No. of Patients (eyes)		368 (736)	471 (932)	/
No. Of OCT scans		736	932	/
Age (yrs), Mean(SD)		70.38 (9.07)	68.72 (8.51)	0.99
Sex	male(%)	148 (40.15%)	135 (28.68%)	0.00
	female(%)	220 (59.85%)	336 (71.32%)	
Eye	right(%)	197 (53.57%)	225 (47.83%)	0.65
	left(%)	171 (46.43%)	246 (52.17%)	
BCVA (LogMAR), Mean (SD)		4.60 (0.28)	4.43 (0.83)	0.00
IOP (mmHg), Mean (SD)		14.88 (3.02)	15.68 (4.39)	0.19

No.: number; SD: standard deviation; /: not available; BCVA: best corrected visual acuity; MAR: minimum angle resolution; IOP: intraocular pressure

subjects came from Northwest China, accounting for 69.60%, and 30.40% came from other regions (Fig. 3). The patients' information: 50 ~ 88 years old; 283 males, 556 females; 442 cases of right eye, 417 cases of left eye, and more details were shown in Table 2. The patients were divided into the normal control group and the PACS group according to the the criterion mentioned above (Fig. 4). There were not any statistical differences in age, gender, and IOP pressure between the two groups

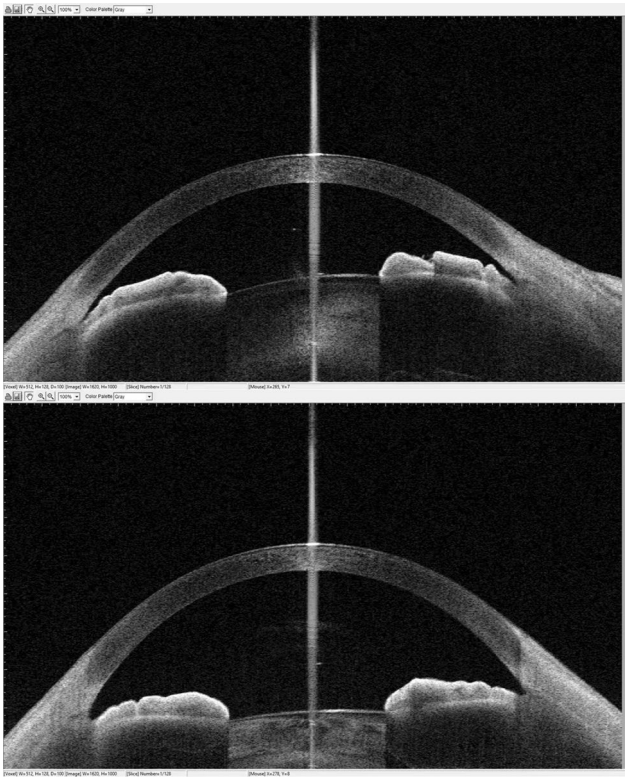

Fig. 4 The representative AS-OCT images of PACS (upper) and healthy control (below)

($P>0.05$), but there were significant differences in gender and visual acuity ($P<0.05$) (Table 2).

Anterior chamber measurement and anatomy analysis

ACD, CCT, ACW, and LV were located in the axial position of anterior chamber, these values held stable in all sites. AOD500, AOD750, ARA500, ARA750, TISA500, TISA750, TIA500, and TIA750 were located in the angle of anterior chamber, and these values were mutative in different sites. The parameters representing the distance of anterior chamber were AOD500 and AOD750. The values at 0° site were slightly larger than 180° site, but there was no statistical difference ($P>0.05$) (Table 3); TIA500 and TIA750 represented the angle of anterior chamber. The value at 0° site was slightly larger than 180° site, and the comparison showed no significant difference ($P>0.05$) (Table 3). The four parameters ARA500, ARA750, TISA500, TISA750 indicated the area of anterior chamber. The mean values of the two group were equal, with no significant differences ($P>0.05$) (Table 3). Overall, the values of angle had no statistical difference at 180° sites and 0° sites (Table 3). In normal group and PACS group, all parameters were statistically different. ACD, ACW, AOD500, AOD750, ARA500, ARA750, TISA500, TISA750, TIA500, and TIA750 in normal group were significantly higher than those in PACS

Table 3 Angle parameters measured by AS-OCT in 180° site and 0° site

	180°	0°	*P* Value
AOD500	0.27 ± 0.18	0.28 ± 0.19	0.39
AOD750	0.38 ± 0.24	0.39 ± 0.25	0.29
ARA500	0.16 ± 0.10	0.16 ± 0.10	0.56
ARA750	0.24 ± 0.15	0.24 ± 0.16	0.87
TISA500	0.12 ± 0.07	0.12 ± 0.08	0.87
TISA750	0.21 ± 0.12	0.21 ± 0.13	0.83
TIA500	18.35 ± 11.09	19.06 ± 11.70	0.16
TIA750	19.20 ± 11.00	19.80 ± 11.14	0.14

AOD500: angle opening distance at 500 μm; AOD750: angle opening distance at 750 μm; ARA500: angular recess area at 500 μm; ARA750: angular recess area at 750 μm; TISA500: trabecular iris space area at 500 μm; TISA750: trabecular iris space area at 750 μm; TIA500: trabecular-iris angle at 500 μm; TIA750: trabecular-iris angle at 750 μm

Table 4 Anterior segment parameters measured by AS-OCT in PACS and normal control group

	Normal Group	PACS Group	*P* Value	AUC(95%CI)
ACD	2.50 ± 0.38	1.86 ± 0.23	0	0.9217(0.8803–0.9632)
ACW	11.25 ± 0.41	10.96 ± 0.46	0	0.6652(0.5742–0.7563)
LV	0.39 ± 0.31	0.90 ± 0.24	0	0.9003(0.8495–0.9511)
CCT	0.52 ± 0.03	0.53 ± 0.03	0.03	0.6033(0.5129–0.6938)
AOD500	0.33 ± 0.18	0.11 ± 0.09	0	0.8853(0.8509–0.9197)
AOD750	0.46 ± 0.23	0.16 ± 0.11	0	0.8927(0.8601–0.9253)
ARA500	0.18 ± 0.10	0.07 ± 0.06	0	0.8369(0.7909–0.8830)
ARA750	0.29 ± 0.15	0.11 ± 0.08	0	0.8630(0.8231–0.9030)
TISA500	0.14 ± 0.07	0.06 ± 0.04	0	0.8554(0.8150–0.8958)
TISA750	0.24 ± 0.12	0.09 ± 0.06	0	0.8767(0.8409–0.9125)
TIA500	22.18 ± 10.42	7.83 ± 6.34	0	0.8859(0.8495–0.9223)
TIA750	22.91 ± 10.12	8.49 ± 5.44	0	0.8995(0.8674–0.9316)

AUC: area under the curve; CI: confidence interval; CCT: central corneal thickness; ACD: anterior chamber depth; ACW: anterior chamber width: LV: lens vault; AOD500: angle opening distance at 500 μm; AOD750: angle opening distance at 750 μm; ARA500: angular recess area at 500 μm; ARA750: angular recess area at 750 μm; TISA500: trabecular iris space area at 500 μm; TISA750: trabecular iris space area at 750 μm; TIA500: trabecular-iris angle at 500 μm; TIA750: trabecular-iris angle at 750 μm

group ($P<0.001$); LV and CCT in the normal control group were significantly smaller than those the PACS group ($P<0.001$) (Table 4). Additionally, all AUC values of these parameters were >0.5, the order from high to low was: ACD, LV, TIA750, AOD750, TIA500, AOD500, TISA750, ARA750, TISA500, ARA500, ACW and CCT (AUC=0.9217, 0.9003, 0.8995, 0.8927, 0.8859, 0.8853, 0.8767, 0.8630, 0.8554, 0.8369, 0.6652, 0.6033, respectively) (Table 4; Fig. 5).

Performance of three machine learning algorithms in test set

The Se of CART, RF, LR achieved 0.76 (95%CI: 0.68–0.84), 0.84 (95%CI: 0.80–0.89) and 0.68 (95%CI: 0.61–0.76), respectively, and the Sp achieved 0.93 (95%CI: 0.68–0.84), 0.92 (95%CI: 0.86–0.97) and 0.91 (95%CI: 0.84–0.97), respectively. The PPV of CART, RF, LR

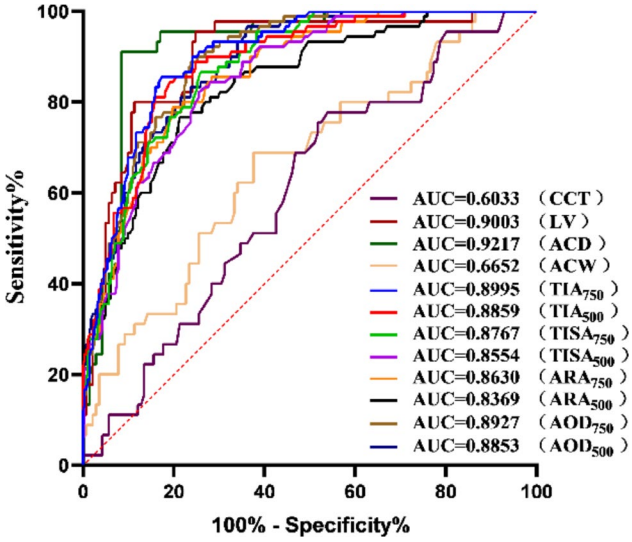

Fig. 5 The AUC values of different chamber parameters. The order from high to low: ACD, LV, TIA750, AOD750, TIA500, AOD500, TISA750, ARA750, TISA500, ARA500, ACW, CCT. AUC: area under the curve; ACD: anterior chamber depth; ACW: anterior chamber width: AOD500: angle opening distance at 500 μm; AOD750: angle opening distance at 750 μm; ARA500: angular recess area at 500 μm; ARA750: angular recess area at 750 μm; CCT: central corneal thickness; LV: lens vault; TISA500: trabecular iris space area at 500 μm; TISA750: trabecular iris space area at 750 μm; TIA500: trabecular-iris angle at 500 μm; TIA750: trabecular-iris angle at 750 μm

Table 5 Se, Sp, PPV, NPV, AUC of traditional machine learning algorithms

	Se (95%CI)	Sp (95%CI)	PPV (95%CI)	NPV (95%CI)	AUC (95%CI)
CART	0.76 (0.68,0.84)	0.93 (0.87,0.99)	0.85 (0.74,0.95)	0.92 (0.90,0.95)	0.90 (0.85,0.92)
RF	0.84(0.80,0.89)	0.92 (0.86,0.97)	0.82 (0.70,0.93)	0.95 (0.93,0.96)	0.91 (0.86,0.96)
LR	0.68(0.61,0.76)	0.91 (0.84,0.97)	0.79 (0.66,0.92)	0.90 (0.88,0.92)	0.86 (0.79,0.93)

Se: sensitivity; Sp: Specificity; PPV: positive predict value; NPV: negative predict value; AUC: area under the curve; CART: classification and regression tree; RF: Random forest; LR: logistic regression

achieved 0.85 (95%CI: 0.74–0.95), 0.82 (95%CI: 0.70–0.93) and 0.90 (95%CI: 0.88–0.92), respectively, and the NPV achieved 0.92 (95%CI: 0.90–0.95), 0.95 (95%CI: 0.93–0.96) and 0.90 (95%CI: 0.88–0.92), respectively. The AUC of RF was 0.91 (CI: 0.86–0.96), better than that of CART (0.90, 95%CI: 0.85–0.92) and that of LR (0.86, 95%CI: 0.79–0.93) (Table 5) (Figs. 6, 7 and 8). The mean of the evaluation indicators of the three models was compared. In the Se comparison, the RF was 0.84, higher than that of the other two groups (Table 5). In the Sp comparison, the CART had a value of up to 0.93 (Table 5). In the comparison of PPV, the CART had a maximum value of 0.85 (Table 5). In the comparison of NPV, the RF was 0.95 higher than the other two groups (Table 5). In the AUC value comparison, the RF had the highest value of 0.91 (Table 5).

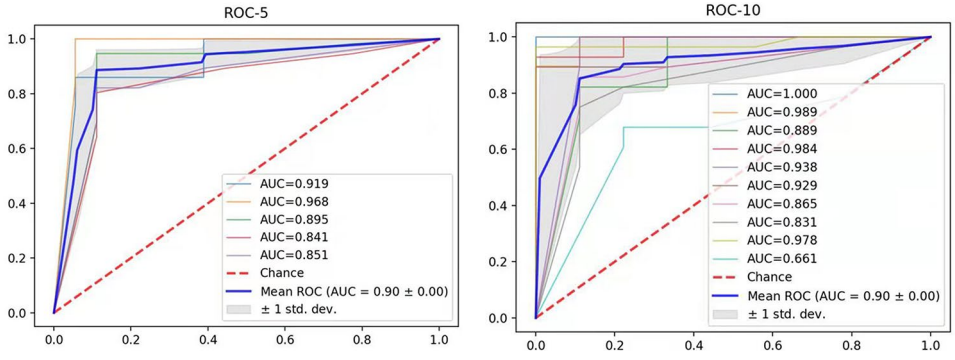

Fig. 6 The AUC value of CART

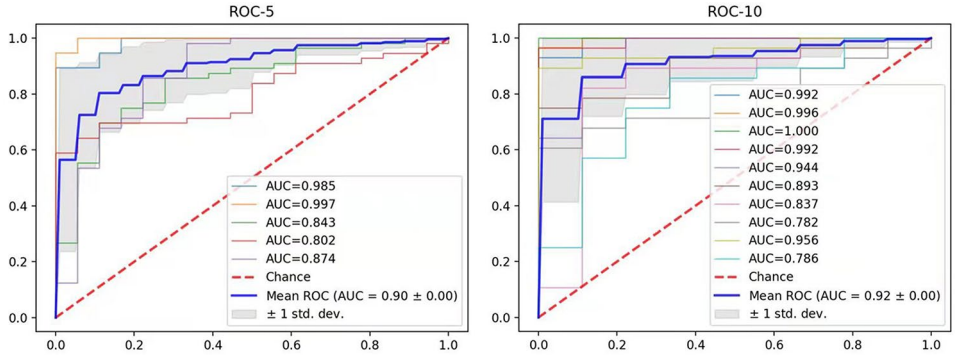

Fig. 7 The AUC value of RF

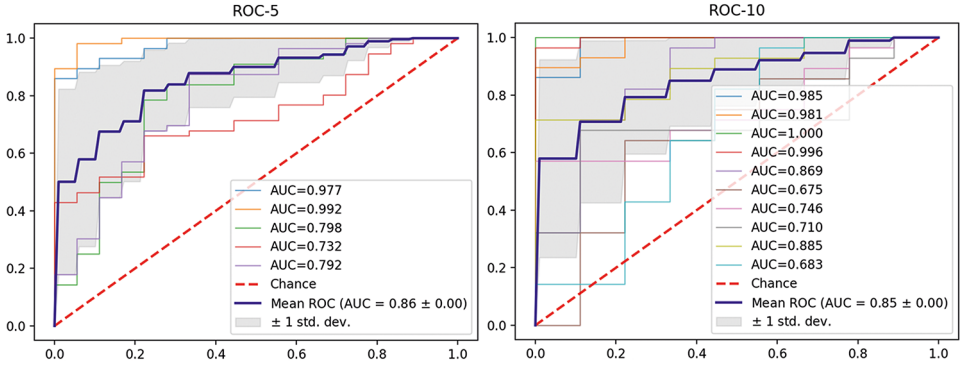

Fig. 8 The AUC value of LR

Performance of two CNN approaches in validation set

The Se of Alexnet and the Se of VGG-16 were similar, which achieved 0.83 (95%CI: 0.74–0.93) and 0.84 (95%CI: 0.74–0.94), respectively. But Sp of Alexnet was better than that of VGG-16, the values reached 0.95 (95%CI: 0.93–0.97), compared with (0.90, 95%CI: 0.85–0.95). The NPV of Alexnet and VGG-16 achieved 0.90 (95%CI: 0.85–0.95) and 0.90 (95%CI: 0.85–0.96), respectively, which showed no significant differences. But for PPV, Alexnet (0.92, 0.89–0.95) was better than VGG-16 (0.85, 95%CI: 0.80–0.90). AUC of Alexnet was 0.85 (95%CI: 0.77–0.92), far better than that of VGG-16 (0.79, 95%CI: 0.74–0.84) (Table 6; Fig. 9).

Comparation of the diagnostic ability between physicians with different experience and different AI models

The Se of junior physicians was 0.71 (95%CI: 0.59–0.85), and the Sp was 0.70 (95%CI: 0.61–0.80), and the PPV was 0.69 (95%CI: 0.54–0.84), and the NPV was 0.71 (95%CI: 0.55–0.87), and AUC was 0.70 (95%CI: 0.62–0.78) (Table 7). These parameters were much inferior to AI models. The mean values of all indexes in the junior physician group were lower than those of the two CNN models, and the difference was statistically significant ($P<0.05$). Comparing the ophthalmologist and the AI models, it was found: the AUC of ophthalmologist was slightly higher than VGG-16, while the Sp, PPV, and NPV

Table 6 Se, Sp, PPV, NPV, AUC of CNN algorithms

		Se	Sp	PPV	NPV	AUC
VGG-16	1	0.83	0.93	0.88	0.9	0.73
	2	0.94	0.86	0.81	0.96	0.79
	3	0.89	0.86	0.8	0.92	0.82
	4	0.83	0.93	0.88	0.9	0.82
	5	0.72	0.93	0.87	0.84	0.79
	M (95%CI)	0.84 (0.74,0.94)	0.90 (0.85,0.95)	0.85 (0.80,0.90)	0.90 (0.85,0.96)	0.79 (0.74,0.84)
Alexnet	1	0.89	0.93	0.89	0.93	0.81
	2	0.89	0.93	0.89	0.93	0.94
	3	0.89	0.96	0.94	0.93	0.8
	4	0.72	0.96	0.93	0.84	0.86
	5	0.78	0.96	0.93	0.87	0.82
	M (95%CI)	0.83 (0.74,0.93)	0.95 (0.93,0.97)	0.92 (0.89,0.95)	0.90 (0.85,0.95)	0.85 (0.77,0.92)

Se: sensitivity; Sp: Specificity; PPV: positive predict value; NPV: negative predict value; AUC: area under the curve; CNN: convolutional neural network; VGG-16: Visual Geometry Group-16

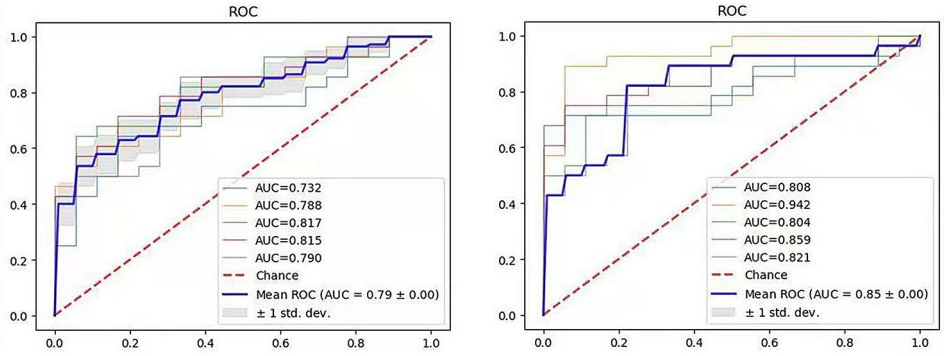

Fig. 9 The AUC value of VGG-16 (left) and Alexnet (right)

Table 7 Performance of junior physicians compared with CNN algorithms

	Se	Sp	PPV	NPV	AUC
Physician 1	0.73	0.75	0.76	0.72	0.74
Physician 2	0.89	0.72	0.64	0.92	0.78
Physician 3	0.68	0.79	0.84	0.6	0.72
Physician 4	0.63	0.65	0.68	0.6	0.64
Physician 5	0.65	0.6	0.52	0.72	0.62
M (95%CI)	0.71 (0.59,0.85)	0.70 (0.61,0.80)	0.69 (0.54,0.84)	0.71 (0.55,0.87)	0.70 (0.62,0.78)
P_1 Value	0.02	0.01	0.06	0.02	0.08
P_2 Value	0.03	0	0.01	0.02	0.01

CNN: convolutional neural network; Se: sensitivity; Sp: Specificity; PPV: positive predict value; NPV: negative predict value; AUC: area under the curve; CNN: convolutional neural network; VGG-16: Visual Geometry Group-16. P1:Comparison between junior physician and VGG-16; P2: Comparison between junior physician and Alexnet

Table 8 Performance of expert ophthalmologists

		Se	Sp	PPV	NPV	AUC
Expert ophthalmologists	1	0.88	0.8	0.81	0.87	0.84
	2	0.8	0.8	0.8	0.8	0.8
	M	0.84	0.8	0.81	0.84	0.82

were far lower than those of VGG-16. Additionally, the Se of ophthalmologist was slightly higher than Alexnet, while the Sp, PPV and NPV were far lower than those of Alexnet (Table 8).

Discussion

During PACG progression, in the stage of PACS, laser iridotomy can prevent seizures of disease effectively and protect the optic nerve to the greatest extent [24]. In addition, some patients with high risk of PAC present with chronic episodes and progressive vision loss [25]. The visual fate of these patients depends on the timing of diagnosis and treatment. Therefore, early screening for high-risk patients is critical. Screening requires easy-to-use instruments and reliable tools for diagnosing. Gonioscopy is a relatively subjective technique, which requires considerable expertise and patient's cooperation [26]. Ultrasound biomicroscopy (UBM) probes anterior segment structures by transmitting and receiving high-frequency ultrasonic pulses; the pressure on the eye caused by the UBM probe, and the water in cup can cause subtle deformation of the anterior segment tissue, which may

lead to a false-negative result of widening of the angle; additionally, due to the risk of infection, UBM is contraindicated in patients who are difficult to cooperate, suffer from open trauma, or postoperative [27]. AS-OCT may be a promising strategy to conduct screening in a large population, because its superiority such as rapid, noninvasive and high resolution [28]. So in the current work, AI models were established and tested based on AS-OCT images. AS shown in Fig. 10. first, general information and anterior chamber parameters were analyzed. After that, three machine learning models were built according to the anterior chamber parameters. Then, two CNN models were established based on the anterior chamber images. Finally, the optimal model was compared with the clinician's diagnostic ability.

The majority of subjects in the dataset were from Shaanxi Province, China. Most of them are women, and over 50 years old. This is consistent with the conclusion of previous epidemiological studies in China: incidence of PACG is gradually increased in people over 50 years old, and women have a higher incidence [29, 30]. Patients with better vision and without clinical symptoms are more likely to be submerged in healthy population, so we selected the majority of patients with normal vision and IOP in the dataset.

The parameters of anterior chamber in PACS group showed different characteristics from those in the normal group. ACD and ACW in the PACS group were smaller than those in the normal group, which were similar to previous reports [31, 32]. LV is a comprehensive index representing the degree of lens thickening or forward relative to scleral spur, and it is an independent predictor of pupillary block [33]. This study showed LV of PACS patients was significantly larger than which of healthy population. PACS group was characterized by a front lens, which is consistent with a previous report [32]. Additionally, it was revealed that CCT of PACS group was slightly larger than normal control group, which also aggravated the crowding of anterior chamber. The angle parameters such as AOD500, AOD750, ARA500, ARA750, TISA500, TISA750, TIA500, and TIA750 in the PACS group were smaller than those in the normal control group, which could probably be resulted from lens advancement, pupillary blocking, and iris bulging [34]. In addition, the difference between the two groups at the parameters at 750 μm was greater than at 500 μm, which is consistent with the phenomenon observed by a previous study [35].

According to ROC, all of the 12 parameters are meaningful for disease diagnosis. ACD and LV have the highest

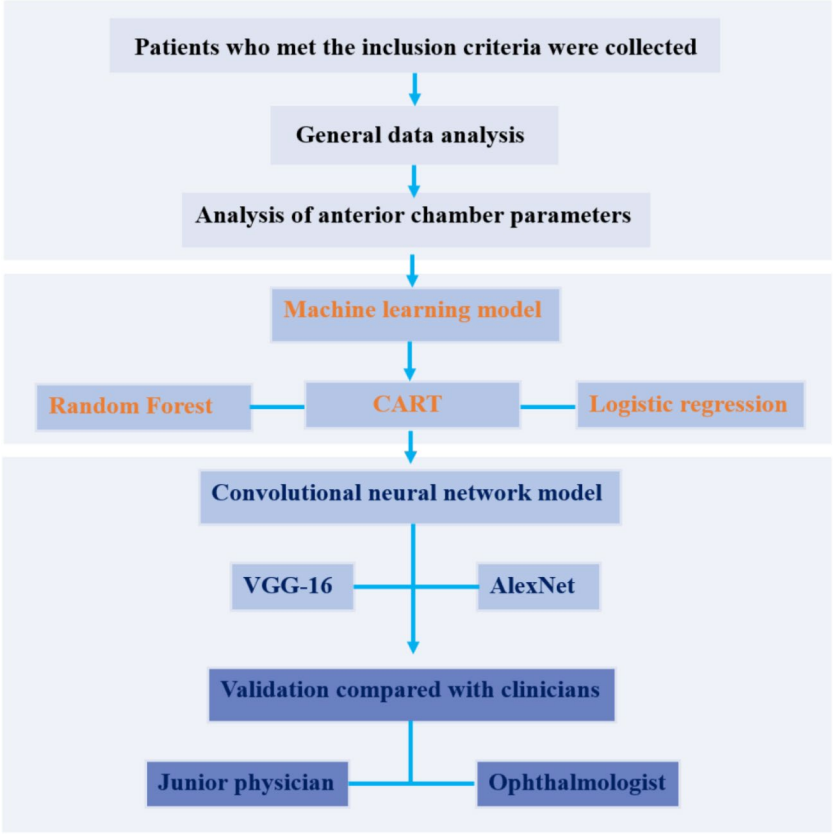

Fig. 10 Overall framework of the proposed approach

values. LV is regarded as the most valuable indicator for distinguishing mature cataract and angle closure in Asia [36, 37]. ACD is the most accessible indicator, many studies have used it to establish threshold standards for angle closure risk [38, 39]. The parameters reflecting angle and distance have greater diagnostic value, while the parameters reflecting area have a slightly worse diagnostic value. A previous study reports that the AUC values of anterior chamber parameters, from high to low, were: AOD750, AOD500, TISA750, ARA750, TISA500 [40], and the order is completely consistent with our study. Its indicates the angle parameters are stable and repeatable in diagnosing angle closure. The diagnostic value of area is not as strong as distance and angle. Because the degree of iris moving forward is affected by morphology and attachment points of root. When angle is narrow or closed, the deformation of corner has a buffer space, and the narrowing of the area doesn't happen immediately [41]. Parameters at 750 μm generally have higher diagnostic value than 500 μm because they are more sensitive and less affected by iris surface morphology. Compared with others, the significance of ACW and CCT is relatively weak in diagnosing PACS, which is consistent with a previous report [42].

Recently, a study reports that three machine learning models were established by anterior chamber parameters for the diagnosis of PACS, and the AUC reached a high level, but Se and Sp were lower than 0.8 [43]. Those weren't qualified for population screening, probably because three mechanisms of angle-closure were included (pupillary block, plateau iris configuration and thick peripheral iris roll). Afterwards, the team found those models were more suitable for populations with pupillary block [44]. In this study, PACS group was mainly composed of angle-closure cases with pupillary block. The value of Sp were better than these reports mentioned above [43, 44], but the value of Se and AUC were inferior. The reason might be the influence of iris root on anterior chamber angle was not considered in light or dark environments. In this study, we found LR cannot handle multiple parameters well, and the diagnostic ability is poor. CART and RF showed their own outstanding merit.

In these models, we found RF had high value of Se, NPV, and AUC, and CART had high value of Sp and PPV. In practically screening, missed diagnosis rate is a more serious error than misdiagnosis rate, and the goal of model training is to improve diagnostic sensitivity and avoid patients being missed [45]. In addition, the comprehensive diagnostic ability of RF is stronger. Therefore, RF is the best candidate of parametric models. A previous study established a VGG-16 model with 39,936 scans of anterior segment images to diagnose angle closure, and the AUC was 0.85, sensitivity was 0.83, and specificity was 0.87 [46]. Compared with PAC or PACG, the anatomical structure of PACS is closer to normal anterior chamber, so diagnosis of PACS is more difficult. However, in this study, the diagnostic performance of VGG-16 and Alexnet is better than the above study. Although VGG-16 has slight advantage in NPV and Se, Alexnet has significant advantage in Sp, PPV, and AUC. Generally, the Se increased, the Sp decreased. The threshold parameters of models should to be customized according to different scenarios. we should program models to ensure the diseases are not missed, it will not cause too much false negative cases [47]. However, VGG-16 showed high false-positive rate, it may bring patients' panic, suspicion, and disgust for screening, it also caused waste of medical resources, which will make the screening effect reduced greatly. In contrast, in our opinion, Alexnet is more conducive for promotion and implementation of screening projects.

It is reported that, ResNet-50 surpasses all scoring physicians in accuracy of diagnosing, and surpasses all ophthalmologists who as reference standard in repeatability [48]. This study reached similar conclusions. Junior doctors' performances were inferior than AI model in diagnostic indicators. We compared diagnostic results of ophthalmologists with AI, and found VGG-16 and Alexnet reached the level of ophthalmologists in diagnostic capabilities, which can be a reliable auxiliary tools for PACS screening and diagnosis, especially in community. Our findings also suggest that, deep learning may also be a promising teaching tool to promote the diagnostic ability of young physicians.

This study has some limitations. This study was used for angle screening of PACG high-risk groups, without considering interpretation of fundus and visual field. The positive cases should be referred to ophthalmology hospital for further diagnosis. The number of patients is also limited, and most of whom came from Shaanxi province, and more patients from medical centers of different regions should be enrolled, which will further validate the values of these models. The suitable strategies to screen the subjects with plateau iris configuration and thick peripheral iris roll are also necessary to be explored in the future. More extensive, multi-type, and multi-center data will be included in frame of AI models. From a technical point of view, data augmentation techniques like CutMix, MixUp, and AutoAugment may help improve the performance of CNN models, which may be explored in the following work. Increasing studies have indicated that other CNN architectures, such as EfficientNet, ResNet and MixNet, have their respective advantages in making diagnosis based on medical images [49, 50]. These approaches are also needed to be compared in the following work.

Conclusion

In this study, we provide an early screening strategy for PACS based on AS-OCT images. AI-assisted diagnosis of PACS is credible, and it is expected to become a clinical auxiliary tool for early glaucoma screening in the future. Additionally, deep learning may improve the diagnostic ability of young physicians.

Acknowledgements
Clinical Research Center for Ophthalmic Diseases of Shaanxi Province, Sanqin Talent Special Support Plan Innovation and Entrepreneurship team, Education Department of Shaanxi Provincial Government for Pathogenesis and Prevention Transformation Medicine for Glaucoma Innovation Team, Clinical Key Specialty of Shaanxi Province, Xi'an International Science and Technology Cooperation Base for Ophthalmology and Visual Science, Xi'an Key Laboratory for the Prevention and Treatment of Eye and Brain Neurological Related Diseases, Ophthalmology Science and Technology Innovation Team of Xi'an Medical University, and Key Disciplines of Xi'an Medical University provided support for the present work. The authors also thank Jian Zhang, Zhonglan Guo, Weiwei Wang, Junxia Zhang, Xia Wang, Xin Gao, Xiangxiang Yang, Ying Liu, Xu Liu, Ruixue Zhang, Zhuoya Quan, Beilei He, Yao Lu, Dandan Liu, Jie Yang for their contribution in the data collection of this study.

Author contributions
M.Z., J.F. & Y.H. designed the study. Z.F., J.X., Z.J., J.W., R.S., X.P., J.Y., F.X., J.L., Y.W. & H.Z. colletected the clinical data. R.Z., M.Z. & J.F. developed the AI models; Z.F., J.X. & Z.J. drafted the manuscript; Y.H. reviewed the manuscript. All authors agree with the final version of the manuscript.

Funding
This work was supported by the National Natural Science Foundation of China (grant no.82070964), Shaanxi Science Fund for Distinguished Young Scholars (No.2022JC-60) the International Scientific and Technological Cooperation Projects (No.2024GH-YBXM-20), The Open Research Funds of the State Key Laboratory of Ophthalmology (No. 83000-32030002), and Education Department of Shaanxi Provincial Government for Youth Innovation Team Research Program Project (No.23JP151 and (No.23JP150). This work was also partly financially supported by the Key R&D Plan of Shaanxi Province, China (No.2023-YBSF-304).

Data availability
The codes for the machine learning algorithms and deep learning algorithms are provided in https://github.com/xiandrheyuan/PACS_DL and https://github.com/xiandrheyuan/PACS respectively. More details of the study design, algorithms and labeled OCT images are available from the corresponding author upon request.

Declarations

Ethics approval and consent to participate
This study included human subjects. All participants signed informed consents. The study was approved by The Second Affiliated Hospital of Xi'an Medical University, performed in accordance with the Declaration of Helsinki. All authors have no proprietary or commercial interest in any materials discussed in this article.

Consent for publication
Not applicable.

Competing interests
The authors declare no competing interests.

Received: 24 February 2024 / Accepted: 29 August 2024
Published online: 09 September 2024

References

1. Sun X, Dai Y, Chen Y, Yu DY, Cringle SJ, Chen J, Kong X, Wang X, Jiang C. Primary angle closure glaucoma: what we know and what we don't know. Prog Retin Eye Res. 2017;57:26–45.
2. Tham YC, Li X, Wong TY, Quigley HA, Aung T, Cheng CY. Global prevalence of glaucoma and projections of glaucoma burden through 2040: a systematic review and meta-analysis. Ophthalmology. 2014;121(11):2081–90.
3. Cheng JW, Zong Y, Zeng YY, Wei RL. (2014). The prevalence of primary angle closure glaucoma in adult asians: a systematic review and meta-analysis. PLoS ONE, 9(7), e103222.
4. Foster PJ, Buhrmann R, Quigley HA, Johnson GJ. The definition and classification of glaucoma in prevalence surveys. Br J Ophthalmol. 2002;86(2):238–42.
5. Potop V, Corbu C, Coviltir V, Schmitzer S, Constantin M, Burcel M, Ionescu C, Dascalescu D. The importance of corneal assessment in a glaucoma suspect - a review. Rom J Ophthalmol. 2019;63(4):321–6.
6. Singh K, Singh A, Bhattacharyya M. Iris clues in ACG. Int Ophthalmol. 2021;41(5):1959–64.
7. Wang X, Chen X, Tang Y, Wang J, Chen Y, Sun X. Morphologic Features of Crystalline Lens in patients with primary Angle Closure Disease observed by CASIA 2 Optical Coherence Tomography. Investig Ophthalmol Vis Sci. 2020;61(5):40.
8. Moghimi S, Torkashvand A, Mohammadi M, Yaseri M, Saunders LJ, Lin SC, Weinreb RN. (2018). Classification of primary angle closure spectrum with hierarchical cluster analysis. PLoS ONE, 13(7), e199157.
9. He M, Jiang Y, Huang S, Chang DS, Munoz B, Aung T, Foster PJ, Friedman DS. Laser peripheral iridotomy for the prevention of angle closure: a single-centre. Randomised Controlled Trial Lancet. 2019;393(10181):1609–18.
10. Momont AC, Mills RP. Glaucoma screening: current perspectives and future directions. Semin Ophthalmol. 2013;28(3):185–90.
11. Razeghinejad MR, Myers JS. Contemporary approach to the diagnosis and management of primary angle-closure disease. Surv Ophthalmol. 2018;63(6):754–68.
12. Porporato N, Baskaran M, Husain R, Aung T. Recent advances in anterior chamber angle imaging. Eye. 2020;34(1):51–9.
13. Gupta N, Varshney A, Ramappa M, Basu S, Romano V, Acharya M, Gaur A, Kapur N, Singh A, Shah G, Chaudhary I, Patel N, Tiwari A, Kate A, Sangwan V, Mathur U. Role of AS-OCT in managing corneal disorders. Diagnostics. 2022;12(4):918. https://doi.org/10.3390/diagnostics12040918.
14. Maria A, Ablameyko S. AI image-based diagnosis systems: how to implement them? J Digit Health. 2023;2(1):12–21.
15. Pasa F, Golkov V, Pfeiffer F, Cremers D, Pfeiffer D. Efficient Deep Network architectures for fast chest X-Ray tuberculosis screening and visualization. Sci Rep. 2019;9(1):6268.
16. Yang G, Li K, Yao J, Chang S, He C, Lu F, Wang X, Wang Z. Automatic measurement of anterior chamber angle parameters in AS-OCT images using deep learning. Biomedical Opt Express. 2023;14(4):1378–92.
17. Fu H, Xu Y, Lin S, Wong D, Baskaran M, Mahesh M, Aung T, Liu J. Angle-Closure detection in anterior segment OCT based on Multilevel Deep Network. Ieee Trans Cybernetics. 2020;50(7):3358–66.
18. Jaworski M, Duda P, Rutkowski L, Jaworski M, Duda P, Rutkowski L, Rutkowski L, Duda P, Jaworski M. New splitting criteria for decision trees in Stationary Data streams. Ieee Trans Neural Networks Learn Syst. 2018;29(6):2516–29.
19. Rau CS, Wu SC, Chien PC, Kuo PJ, Chen YC, Hsieh HY, Hsieh CH, Liu HT. (2018). Identification of pancreatic Injury in patients with elevated amylase or lipase level using a decision Tree Classifier: a cross-sectional retrospective analysis in a level I trauma Center. Int J Environ Res Public Health, 15(2).
20. Yang L, Wu H, Jin X, Zheng P, Hu S, Xu X, Yu W, Yan J. Study of cardiovascular disease prediction model based on random forest in eastern China. Sci Rep. 2020;10(1):5245.
21. Hess AS, Hess JR. Logistic Regres Transfus. 2019;59(7):2197–8.
22. Guan Q, Wang Y, Ping B, Li D, Du J, Qin Y, Lu H, Wan X, Xiang J. Deep convolutional neural network VGG-16 model for differential diagnosing of papillary thyroid carcinomas in cytological images: a pilot study. J Cancer. 2019;10(20):4876–82.
23. Kanimozhi VS, Balasubramani M, Anuradha R. Hierarchal Bayes model with Alexnet for characterization of M-FISH chromosome images. Med Biol Eng Comput. 2021;59(7–8):1529–44.
24. Tanner L, Gazzard G, Nolan WP, Foster PJ. Has the EAGLE landed for the use of clear lens extraction in angle-closure glaucoma? And how should primary angle-closure suspects be treated? Eye. 2020;34(1):40–50.

25. Ong EL, Baasanhu J, Nolan W, Uranchimeg D, Lee PS, Alsbirk PH, Johnson GJ, Foster PJ. The utility of symptoms in identification of primary angle-closure in a high-risk population. Ophthalmology. 2008;115(11):2024–9.
26. Kurysheva NI, Sharova GA. Primary anterior chamber angle closure: progression from suspect to glaucoma. Part 1. Frequency and rate of transition from suspected primary angle closure to true angle closure and primary angle closure glaucoma. Vestn Oftalmol. 2022;138(4):101–7.
27. Pei XT, Wang SH, Sun X, Chen H, Wang BS, Li SN, Wang T. Predictors of angle widening after laser iridotomy in Chinese patients with primary angle-closure suspect using ultrasound biomicroscopy. (2022), *Int J Ophthalmol*. 2022;15(2):233–241.
28. Chakrabarti K, Samant S, Mohapatra R, Mishra S, Das S, Chakrabarti M. A comparison of lens parameters in patients with various subtypes of primary angle-closure disease and the normal population: a prospective study. Indian J Ophthalmol. 2022;70(8):2889–94.
29. Wang L, Huang W, Huang S, Zhang J, Guo X, Friedman DS, Foster PJ, He M. Ten-year incidence of primary angle closure in elderly Chinese: the Liwan Eye Study. Br J Ophthalmol. 2019;103(3):355–60.
30. Zhu J, Xu Y, Wang H, Liu D, Zhu J, Wu H. The seasonality of Acute Attack of Primary Angle-Closure Glaucoma in Beijing. China Sci Rep. 2018;8(1):4036.
31. He M, Huang W, Zheng Y, Alsbirk PH, Foster PJ. Anterior chamber depth in elderly Chinese: the Liwan eye study. Ophthalmology. 2008;115(8):1286–90.
32. Nongpiur ME, Sakata LM, Friedman DS, He M, Chan YH, Lavanya R, Wong TY, Aung T. Novel association of smaller anterior chamber width with angle closure in singaporeans. Ophthalmology. 2010;117(10):1967–73.
33. Nongpiur ME, He M, Amerasinghe N, Friedman DS, Tay WT, Baskaran M, Smith SD, Wong TY, Aung T. Lens vault, thickness, and position in Chinese subjects with angle closure. Ophthalmology. 2011;118(3):474–9.
34. Wang W, Song H, Liu Z. Computational study on the Biomechanics of Pupil Block Phenomenon. Biomed Res Int. 2019;2019:4820167.
35. Shabana N, Aquino MC, See J, Ce Z, Tan AM, Nolan WP, Hitchings R, Young SM, Loon SC, Sng CC, Wong W, Chew PT. Quantitative evaluation of anterior chamber parameters using anterior segment optical coherence tomography in primary angle closure mechanisms. Clin Experimental Ophthalmol. 2012;40(8):792–801.
36. Tan GS, He M, Zhao W, Sakata LM, Li J, Nongpiur ME, Lavanya R, Friedman DS, Aung T. Determinants of lens vault and association with narrow angles in patients from Singapore. Am J Ophthalmol. 2012;154(1):39–46.
37. Mansouri M, Ramezani F, Moghimi S, Tabatabaie A, Abdi F, He M, Lin SC. Anterior segment optical coherence tomography parameters in phacomorphic angle closure and mature cataracts. Investig Ophthalmol Vis Sci. 2014;55(11):7403–9.
38. Aung T, Nolan WP, Machin D, Seah SK, Baasanhu J, Khaw PT, Johnson GJ, Foster PJ. Anterior chamber depth and the risk of primary angle closure in 2 east Asian populations. Arch Ophthalmol. 2005;123(4):527–32.
39. Saxena S, Agrawal PK, Pratap VB, Nath R. Anterior chamber depth and lens thickness in primary angle-closure glaucoma: a case-control study. Indian J Ophthalmol. 1993;41(2):71–3.
40. Narayanaswamy A, Sakata LM, He MG, Friedman DS, Chan YH, Lavanya R, Baskaran M, Foster PJ, Aung T. Diagnostic performance of anterior chamber angle measurements for detecting eyes with narrow angles: an anterior segment OCT study. Arch Ophthalmol. 2010;128(10):1321–7.
41. Xu BY, Pardeshi AA, Shan J, DeBoer C, Moghimi S, Richter G, McKean-Cowdin R, Varma R. Effect of Angle narrowing on Sectoral Variation of Anterior Chamber Angle Width: the Chinese American Eye Study. Ophthalmol Glaucoma. 2020;3(2):130–8.
42. Leung CK, Palmiero PM, Weinreb RN, Li H, Sbeity Z, Dorairaj S, Leung D, Liu S, Liebmann JM, Congdon N, Lam DS, Ritch R. Comparisons of anterior segment biometry between Chinese and caucasians using anterior segment optical coherence tomography. Br J Ophthalmol. 2010;94(9):1184–9.
43. Zhang Y, Zhang Q, Li L, Thomas R, Li SZ, He MG, Wang NL. Establishment and Comparison of Algorithms for Detection of Primary Angle Closure Suspect based on static and dynamic anterior segment parameters. Translational Vis Sci Technol. 2020;9(5):16.
44. Zhang Y, Dong Z, Zhang Q, Li L, Thomas R, Li SZ, He MG, Wang NL. Detection of primary angleclosure suspect with different mechanisms of angle closure using multivariate prediction models. Acta Ophthalmol. 2021;99(4):e576–86.
45. Kim SJ, Cho KJ, Oh S. (2017). Development of machine learning models for diagnosis of glaucoma. PLoS ONE, 12(5), e177726.
46. Porporato N, Tun TA, Baskaran M, Wong D, Husain R, Fu H, Sultana R, Perera S, Schmetterer L, Aung T. Towards 'automated gonioscopy': a deep learning algorithm for 360 degrees angle assessment by swept-source optical coherence tomography. Br J Ophthalmol. 2022;106(10):1387–92.
47. Ting D, Foo VH, Yang L, Sia JT, Ang M, Lin H, Chodosh J, Mehta JS, Ting D. Artificial intelligence for anterior segment diseases: emerging applications in ophthalmology. Br J Ophthalmol. 2021;105(2):158–68.
48. Chiang M, Guth D, Pardeshi AA, Randhawa J, Shen A, Shan M, Dredge J, Nguyen A, Gokoffski K, Wong BJ, Song B, Lin S, Varma R, Xu BY. Glaucoma Expert-Level detection of Angle Closure in Goniophotographs with Convolutional neural networks: the Chinese American Eye Study. Am J Ophthalmol. 2021;226:100–7.
49. Eslami Y, Mousavi KZ, Farzinvash Z, Safizadeh M, Zarei R, Fakhraie G, Vahedian Z, Mahmoudi T, Fadakar K, Beikmarzehei A, Tabatabaei SM. Deep learning-based classification of subtypes of Primary Angle-Closure Disease with Anterior Segment Optical Coherence Tomography. J Glaucoma. 2023;32(6):540–7.
50. Duong LT, Nguyen PT, Iovino L, Flammini M. Automatic detection of Covid-19 from chest X-ray and lung computed tomography images using deep neural networks and transfer learning. Appl Soft Comput. 2023;132:109851.

Publisher's note